Journal of the Earth and Space Physics, Vol. 41, No. 4, 2016, PP. 23-38

Attenuation of Fourier spectra for 2012 Ahar–Varzaghan earthquakes, Northwestern Iran

Samaei, M.[1*], Miyajima, M.[2]and Nojima, N.[3]

1. Postdoctoral Researcher, Graduate School of Natural Science and Technology, Kanazawa University, Kanazawa, Japan
2. Professor, Graduate School of Natural Science and Technology, Kanazawa University, Kanazawa, Japan
3. Professor, Department of Civil Engineering, Gifu University, Gifu, Japan

(Received: 14 Jul 2014, Accepted: 31 Jan 2016)

Abstract

In this research, we have used 102 strong motion recordings from 2012 Ahar-Varzaghan earthquakes (Mw=6.5 and Mw=6.3) to study the form of attenuation of shear wave Fourier amplitude spectra of those two events. The analysis is carried out in a broad-band frequency range from 0.1 to 20 Hz. A bilinear shape for geometrical spreading is assumed based on nonparametric regression of the data. The hinge point of the bilinear shape is around 60 km away from the earthquake source; the geometric spreading forms for the first and second segments are $R^{-0.9}$ and $R^{-0.5}$, respectively. The results of this study show that there is considerable dependency of the rate of geometrical spreading on frequency. If only frequencies above 1 Hz are considered, the first segment of geometrical spreading will have a slope steeper than R^{-1}. In contract, for lower frequencies it has a gentle slope. The associated quality factor for the assumed shape of geometrical spreading (appropriate for frequencies logarithmically spaced between 0.1 to 20 Hz) is $Q(f)=148\ f^{0.62}$. The estimated $Q(f)$ in this study agrees well with the other estimated shear wave quality factors in the region; however, if the whole attenuation model (consisted of geometrical spreading and quality factor) is considered, there will be conspicuous differences between different models.

Keywords: Ahar-Varzaghan earthquakes, Attenuation, Fourier spectra, Geometrical spreading, Northwestern Iran, Quality factor.

1. Introduction

In earthquake hazard assessment, it is important to estimate the expected ground motion as a function of distance and earthquake magnitude. The ground motion at a particular site is influenced by three main components: source, travel path and local site conditions. Source factors include magnitude, fault geometry, stress drop, rupture process and slip distribution on the fault. Travel path effects contain geometrical attenuation, dissipation of seismic energy due to the earth's elasticity and elastic waves scattering in heterogeneous media. Site factor is an amplification and diminution of seismic waves through the local geological units at the recording station. In this study, we address the second of these three main elements (i.e. travel path factors). Estimation of these factors is a step forward in earthquake risk assessment.

On August 11, 2012, two destructive earthquakes occurred 11 minutes apart near two towns of Varzaghan and Ahar in Northwestern Iran; the first with moment magnitude of 6.5 at 12:23 UTC and the second with moment magnitude of 6.3 at 12:34 UTC (Iranian Seismological Center (IRSC)). These events resulted in over 300 deaths and 3000 injuries. These earthquakes have two important implications: first, they are the biggest instrumental events recorded in northwestern Iran and second, they are very well recorded events, being recorded on more than 60 strong motion stations of Iran Strong Motion Network (ISMN) at Hypocenral distances up to more than 200 km (Table 1 and Fig. 1). These strong motion accelerograms have provided excellent database for studying the earthquake parameters in the region.

In this study, regression analysis is performed to determine the attenuation

[*]Corresponding author: E-mail: meghdad.samaei@gmail.com

model for Fourier amplitude spectra of S wave of those two earthquakes. S wave window is chosen for the regression analysis because it includes the strongest shaking and is the most important from engineering point of view. The variation of Fourier amplitude spectra with distance is examined to specify a geometrical spreading function and a frequency dependent *Q* factor. Those estimated path attenuation factors along with source and site factors can be used in stochastic simulation/prediction of strong ground motions like SMSIM (Boore, 2005) or ESXIM (Motazedian and Atkinson, 2005). These predicted/simulated strong ground motions can be employed to develop Ground Motion Prediction Equations (GMPEs) to predict maximum amplitudes of ground motions (i.e., PGA, PGV and response spectra) as function of magnitude and distance (Atkinson and Boore, 1995). In the future research projects, the source factors for those events can be estimated based on the results of this study.

2. Database

The data used in this study were all recorded by Iran Strong Motion Network (ISMN), which have been installed and operated by Building and Housing Research Center (BHRC). The BHRC ground-motion database has been expanded continuously during the past decades due to the new strong-motion stations and occurrence of large earthquakes. So far more than 10000 strong motion records have been obtained by ISMN since its inception in 1973. Currently, this network comprises of 1160 stations with three component digital acceleroraphs in different active seismic regions of the country (Mirzaei Alavijeh et al., 2007; Iran Strong Motion Network (ISMN)).

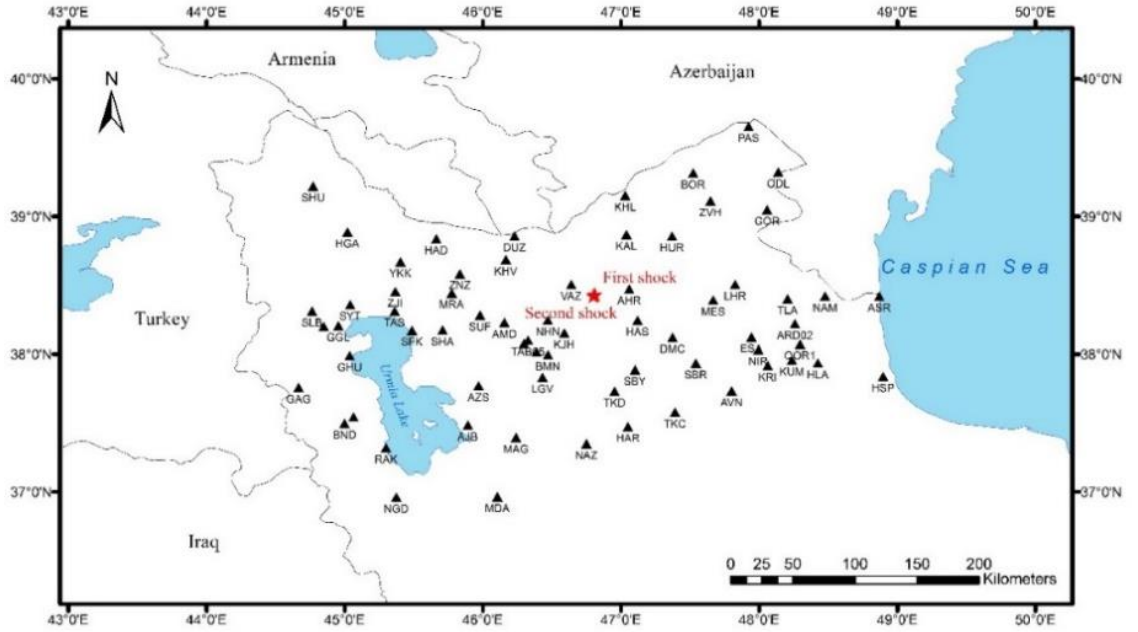

Fig. 1. Location of events and stations. Red stars denote on the location of events and black triangles show the stations. Stars overlap, as the hypocenters of the events are very close.

Table 1. Information of the events

Event	Date	Time	Latitude	Longitude	Depth (km)	Magnitude	Reference	No. of records
First shock	**8/11/2012**	**12:23:15**	**38.433**	**46.812**	**9**	**Mw6.5**	**IRSC**	**49**
Second shock	**8/11/2012**	**12:34:35**	**38.423**	**46.802**	**4**	**Mw6.3**	**IRSC**	**65**

As noted earlier, Ahar-Varzaghan earthquakes have been recorded on more than 60 strong motion stations. They comprised a preliminary database of 114 three component records. All the stations were equipped with three component digital SSA2 accelerographs where the transducer response for them is flat up to 50 Hz. This makes no necessity of correction for instrument response. The sampling rates of the records are 200 Hz (0.005 seconds intervals). It should be noted that the data recorded at the abutments of dams or at the base of buildings have been excluded in three or more stories in height.

Since the magnitudes of these events are greater than 6, it would be appropriate to discuss the features of the strong motion shaking. The biggest PGA in the database occurs at Varzaghan station (VAZ) for the second event, in spite of its moment magnitude being smaller than the first event. The second event is also recorded on more stations compared with the first event. This denotes that the second event is richer in high frequencies. Study of the source spectra of these two earthquakes (Samaei and Miyajima, 2016) confirms this fact as the second event has a higher value of stress drop ($\Delta\sigma$).

Although these earthquakes are recorded with PGA's as high as about 500 cm/s^2, there are actually only a few records passing threshold PGA of 150 to 200, where the nonlinear soil response becomes considerable (Beresnev et al., 1998). Therefore, nonlinear soil response is neglected in the current study.

3. Processing of the records

At first, the data have been visually inspected for quality control and two of them were excluded in this step since they had very short durations (due to late triggering). Then, zero order baseline corrections (Castro et al., 1990; Boore, 1999; Akkar and Bommer, 2006) were applied to all of the records, by subtracting the average of pre-event segment of the records (where is available) or the whole record (where pre-event is not available) from time series. However, we have made no corrections for what we call baseline offsets: small steps or distortions in the reference level of motion, since these effects are important for periods longer than 20 sec (Boore, 1999; Boore, 2001; Boore et al., 2002; Wang et al., 2003) which is not of interest in this study. Another reason for not doing such a procedure is that the results of the method are highly sensitive to choice the baseline correction (The choice of t_2 in Boore, 2001; Boore et al., 2002).

S wave Fourier Amplitude Spectra (FAS) of the acceleration time series were computed using time windows that start with the first arrival of the S wave and end when 90% of the total energy is reached. Time windows were tapered at both ends with a 5% cosine taper before calculation of FAS.

The main issue in our work would be decision making about the bandwidth that data can be used reliably. In high frequencies, decision about maximum frequency that the data are reliable is pretty much easy. At high frequencies, FAS starts to fall toward higher frequencies until it flattens and touches the noise floor (Anderson and Hough, 1984); the data is used for the frequency that FAS touches that floor. This is most recognizable in frequency-FAS plot when frequency is in normal units (not in log units). However, selection of the lowest frequency of data use could be very subjective. In case of digital records, FAS of pre-event segment of the records is usually employed as a model of the noise and the low-cut filter is decided where the signal to noise ratio reaches to some particular value (2 or 3), but this method cannot always be reliable since in low frequencies most of the noise is signal-generated noise and is not present in pre-event portion (Boore and Bommer, 2005). Thus, we have made some criteria to be satisfied together for decision making about lowest usable frequency as follows:

- High signal to noise ratios (Based on pre-event segment): For the records with available pre-event, the ratio of signal to noise should be higher than 3. This criterion is usually satisfied for frequencies as low as 0.1Hz.
- Judgment on the shape of the FAS: According to the theoretical models of the far field Fourier acceleration spectrum (Brune, 1970; Brune, 1971; Atkinson, 1993), an ω^2 decrease is expected in frequencies below the f_c (one corner frequency model) or f_A (two corner frequency model) toward lower frequencies.

A more or less constant amplitude of the FAS at frequencies lower than f_c or f_A generally indicates large low frequency noise (Zaré and Bard, 2002; Boore and Bommer, 2005).

- Visual inspection of velocity and displacement time series after filtering: Acceleration time series are filtered with a low-cut 4th order Butterworth filter with corner frequency of 0.02 Hz. If the integrated velocity and displacement time series of the record after filtering are not "reasonable"(Boore and Bommer, 2005; Akkar and Bommer, 2006), a higher filter corner frequency will be chosen (say 0.03 Hz). This filtering, integrating and inspection is repeated until we get reasonable traces of velocity and displacement. Examples of unreasonable time series could be: velocity or displacement significantly different from zero at the end of the record, long-period fluctuations running along the total record length, long period energy present in P wave of the recording, and etc. Although this method can be somewhat subjective, but it is still the best way to select the lowest frequency of usable bandwidth (David Boore, written communication). Low-cut corner frequencies of the well-known NGA project is selected in the same way (Darragh et al., 2004; Chiou et al., 2008).

Each component of a three component recording may have different freqency band limits. We noticed that at low frequencies, this limit is alike for different components of a recording. However, at high frequencies there is a systematic difference between vertical and horizontal components as vertical components are available at higher frequencies. This is because FAS of vertical components tend to be flattened at much higher frequencies in comparison with the horizontal components. This denotes on higher kappa factor (Anderson and Hough, 1984) for horizontal components. Note that using FAS in a restricted frequency range is equivalent to using band-pass filtered records, which is almost the all needed in processing of strong motion data. The issue as we mentioned is the frequency range that data can be used reliably.

The frequency usable bandwidth for available database is depicted in Figure 2.

FAS is smoothed with a box window with the length of 5 data points and interpolated in 24 logarithmically spaced frequencies between 0.1 to 20 Hz. An example of a record with its raw and interpolated FAS is shown in Figure 3.

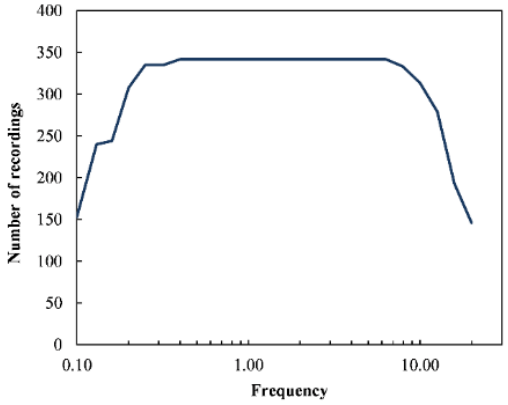

Fig. 2. Number of recordings, available at each frequency for the primary database

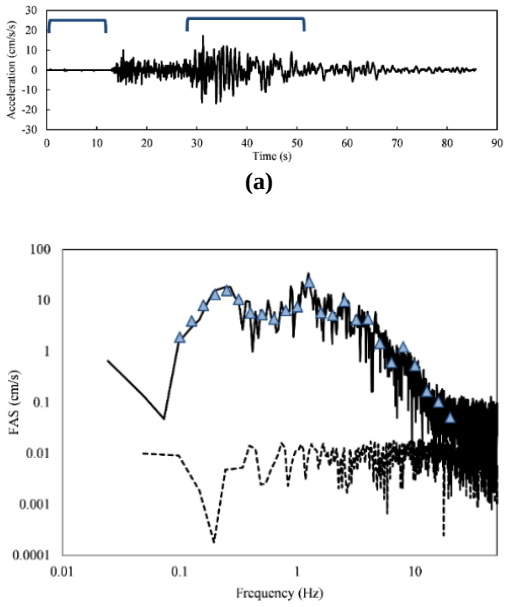

Fig. 3. (a) Vertical component of the first event, recorded at Hadi-Shahr station (HAD) after zero order baseline correction, with its selected noise and S wave windows (hypocentral distance of 110 km). (b) Computed FAS of the S wave (Black line), noise window (dotted line) and smoothed and interpolated FAS of S wave used in regression (triangles). FAS of the noise is normalized to the length of the S wave window by multiplying by the factor $(Tu/Tn)^{1/2}$ where Tu and Tn are the durations of the data sample and the noise sample, respectively (Boatwright et al., 1991).

For a particular earthquake at far distances due to variability in source, travel path and site condition, high amplitude records might be included in the dataset while for the same range of distances, low amplitude records might not. This is mostly because the low amplitude data is below triggering threshold of the instrument. For example, in our case, triggering threshold of the instruments is 10 cm/s^2 of acceleration. At distances far enough from the source, for some stations acceleration may get to 10 cm/s^2 while not for the others (due to the mentioned variability). If only the larger motions were included, this would lead to a bias in the predicted distance decay of the ground motion and there would be a tendency for the predicted ground motions to decay less rapidly with distance than the real data. Therefore, the data need to be truncated at some particular distance, depending on the earthquake magnitude. Joyner and Boore (1981) noticed such a potential bias for the first time to derive ground motion prediction equations for western North America. Joyner and Boore (1981) avoided such a bias by restricting the data to the distances that there is an operating un-triggered station, a scheme that was used by their follow-up works (i.e., Boore et al., 1997). However, in case of Ahar-Varzaghan earthquakes, there are some very close operating un-triggered stations (for unknown reason) which make us unable to use such a procedure. Therefore, following Macias et al. (2008), we have decided distance truncation of the data based on plots like those of Figure 4. As it is seen, amplitudes decay toward longer distances until they touch a floor and do not decay anymore. Based on such plots, while it is noted that the problem is less severe for vertical components, it is decided to truncate the data at distance of 180 km for both earthquakes.

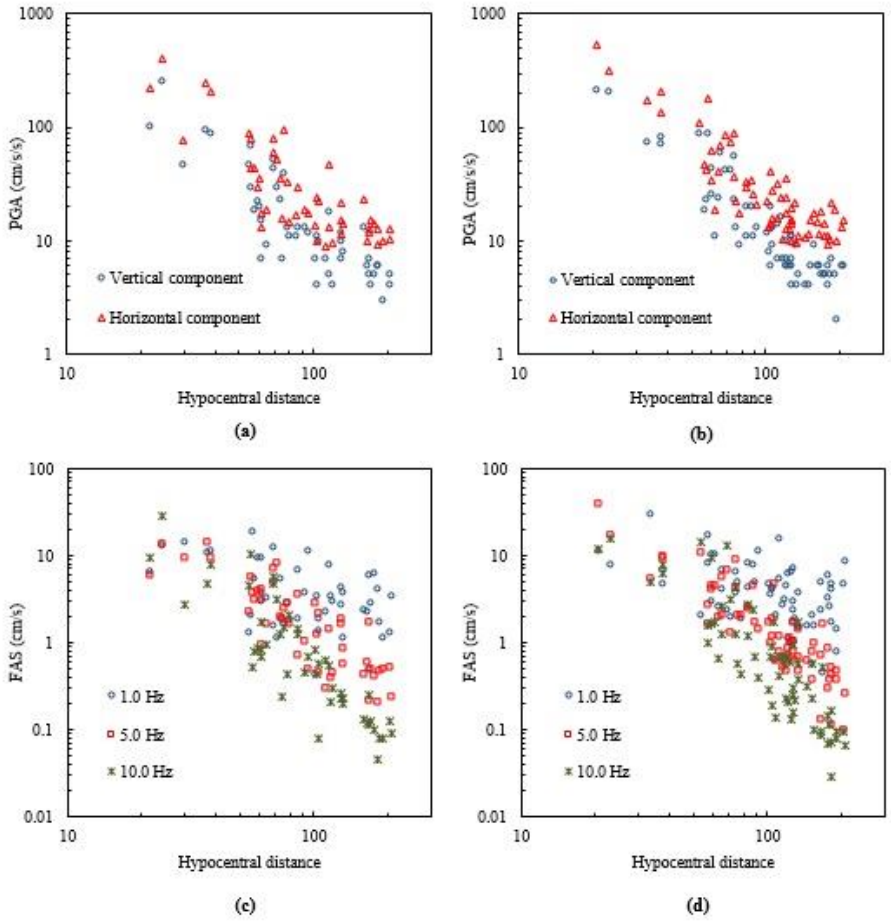

Fig. 4. (a, b) PGA and (c, d) FAS as a function of hypocentral distance. Figures (a, c) are related to the first and figures (b, d) are related to the second shock. Only FAS for vertical component is shown since the regression will be based on vertical component in this study. Visual estimation of the cutoff distance, from where the flattening effect starts, corresponds to 180 km for both shocks.

4. Regression analysis and results

Assuming a point source, Fourier spectrum of ground motion consists of contributions of source *(E)*, Path *(P)* and local site condition *(G)* (Boore, 1983; Boore, 2003):

$$Y(f,R)=E(f,M)\times P(f,R)\times G(f) \quad (1)$$

where *f* is frequency, *R* is distance, *Y (f,R)* is Fourier spectra (in this study Fourier acceleration spectra) and *M* is moment magnitude. *P (f,R)* is parameterized as:

$$P(f,R)=Z(R)exp\left(\frac{-\pi fR}{\beta Q(f)}\right) \quad (2)$$

where $Z(R)$ is geometrical spreading, β is shearwave velocity and $Q(f)$, the quality factor, is a function that is inversely proportional to anelastic attenuation.

$E(f,M)$ can be represented as an ω^2 source model (Brune, 1970, Brune, 1971) and $G(f)$ can be parametrized to attenuation and diminution. However, $E(f,M)$ and $G(f)$ are not parametrized here since we do not deal with them in this study.

One of the problems with the available data is that for many of the stations, there is not any available information about site condition (this is an unfortunate fact for all the data from IMSN). For the stations included in this study, information about shear wave velocity in the upper layers of the soil is available only for less than half of the stations (Sinaeian et al., 2010). To deal with this problem, it is decided to use vertical component records in the regression, because it is believed that the effect of local site conditions on vertical component of the motion is negligible (Lermo and Chávez-García, 1993). One may recommend using H/V curve as the site term; however, using H/V curve to remove site effects from horizontal components is equivalent to use of vertical components themselves. Thus, we decided to use the vertical components for use in regression in this study. Nevertheless, the model will be checked later to see whether it is appropriate for the horizontal component data or not.

So substituting Equation (2) in Equation (1) without site term gives:

$$Y(f,R)=E(f,M)\times Z(R)exp\left(\frac{-\pi fR}{\beta Q(f)}\right) \quad (3)$$

In this equation, *R* is originally hypocentral distance based on point source representation of ground motion, but it can be modified to account for geometric effects of a finite source (Atkinson and Silva, 2000; Atkinson et al., 2009). In this study, we slightly tried Atkinson and Silva's (2000) coefficients to account for these geometrical effects on *R*, but we observed no important difference between a modified *R* and hypocentral distance. Hence, for available dataset we keep using hypocentral distance as distant measure, for clarity and simplicity.

$Z(R)$ and $Q(f)$ in Equation 3 have trade-offs together; i.e., one cannot be estimated without regarding the other, or they should be estimated simultaneously in the regression. This leads to a relatively weak regression. The other issue is the functional form of geometrical spreading where can be linear, bilinear or trilinear. The classical form of geometrical spreading is a bilinear function (Street et al., 1975; Wang and Herrmann, 1980; Herrmann and Kijko, 1983): this function is:

$$Z(R)=\begin{cases}\dfrac{1}{R} & R\le R_1\\ \dfrac{1}{R_1}\left(\dfrac{R_1}{R}\right)^{0.5} & R>R_1\end{cases} \quad (4)$$

where R_1 is normally fixed at 100 km. The first segment corresponds to geometrical spreading for body waves in a whole-space and the second segment corresponds to theoretical form for surface waves in a half-space. Note that Equation (4) will be composed of two lines with gradients of *-1* and *-0.5* in log-log plot so the term "bilinear" is appropriate.

However, in the past two decades, starting with the work of Atkinson and Mereu (1992), much attention has been paid to the effects of post-critical Moho reflections on the shape of the geometrical spreading. This concentration has mostly led to development of trilinear functional forms of geometrical spreading in different regions around the world (Atkinson, 2004; Motazedian, 2006; Allen et al., 2007; Nayak et al., 2011; Motaghi and Ghods, 2012; Meghdadi and Shoja-Taheri, 2014). These trilinear shapes have a flat or almost flat level as the middle segment. Yet, how effective these trilinear forms really are (given their complexity) is still matter of question (Atkinson, 2012; Boore, 2012; Atkinson and Boore, 2014).

An example of trilinear geometrical spreading which has been used for developing GMPEs in northeastern America is described below (Atkinson and Boore, 1995):

$$Z(R)=\begin{cases}\dfrac{1}{R} & R\le 70km\\ \dfrac{1}{70} & 70\text{ km}<R\le 130km\\ \dfrac{1}{70}\left(\dfrac{130}{R}\right)^{0.5} & R>130km\end{cases} \quad (5)$$

Nonetheless, Babaie Mahani and Atkinson (2012), Atkinson (2012) and Atkinson and Boore (2014) concluded that the bilinear form is the optimal choice:

"The bilinear form strikes the optimal balance between an overly simplistic model and one that accounts for all the complexity in the attenuation behavior. In other words, while there is evidence that the attenuation form is trilinear, at least at lower frequencies, the evidence is not sufficiently compelling to warrant the added complexity of the additional parameters that must be specified for the trilinear form" (Atkinson and Boore, 2014).

Following those studies, we search for an optimal bilinear form of geometrical spreading. To visually find the hinge point for geometrical spreading function, a locally weighted scatterplot smoothing algorithm called Lowess (Cleveland, 1979; Cleveland, 1993) is used. The method uses locally weighted linear regression to smooth the data. The smoothing process is local because it calculates each smoothed value (fitted line) by a set of neighboring data. The smoothing process is weighted because a regression weight function is defined for the data points contained within the data spans.

The available dataset is composed of the records of two earthquakes with the span less than half moment magnitude (M_w=6.5, M_w=6.3). Figure 5 indicates that there is no obvious difference in Fourier amplitude spectra of the two earthquakes and also the way they decay. Using this point, we use Lowess smoothing on the data of both earthquakes together without any scaling for the amplitude levels. This leads to nonparametric plot shown in figure 6.. In this figure it's obvious that the behavior of the amplitude in distance is heavily dependent on the frequency and for each frequency more than one hinge point can be found (Specially for lower frequencies). However, the first obvious hinge points can be found at distance of about 60 or 70 km. Interestingly, hinge points at these distances are in agreement with 1.5 times of the moho depth, where post critical reflections are expected to appear (Moho depth ranges between 38.5 to 53 km in NW Iran as reported by Taghizadeh-Farahmand et al., 2010).

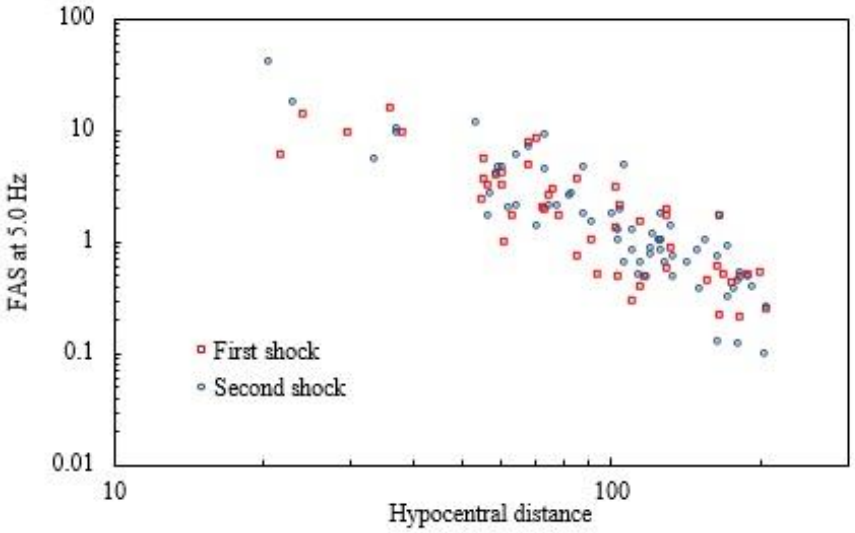

Fig. 5. FAS at 5.0 Hz for both main shocks

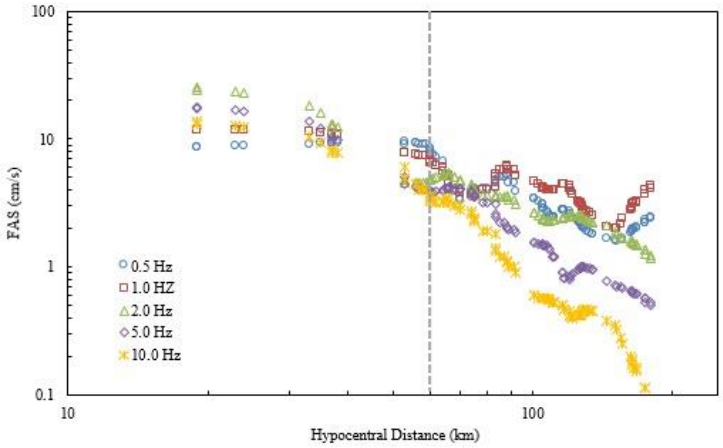

Fig. 6. Nonparametric smoothed FAS of the records. The first hinge point is located at distance of about 60 km. It is obvious from the diagram that high frequencies attenuate more rapidly than low frequencies. This is more apparent for frequencies of 5.0 and 10.0 Hz.

In this study, the distance of 60 km is assumed as the optimal hinge point for segmentation of geometrical spreading. Additionally, the second segment of the geometrical spreading is set to the well-accepted gradient of $1/R^{0.5}$ for regional distances (Herrmann and Kijko, 1983; Atkinson and Mereu, 1992; Raoof et al., 1999; Atkinson, 2004; Motaghi and Ghods, 2012; Atkinson and Boore, 2014), and a preliminary anelastic attenuation term is calculated. Later, using this preliminary anelastic attenuation term for each frequency, gradient of the first segment of geometrical spreading is estimated for close distances ($R \leq 60$km). To determine the preliminary anelastic attenuation term, the Equation (3) in logarithmic form for regional distances is rewritten (R>60km).

$$\log Y_{ij}(f) + 0.5 \log R_{ij} = c_i(f) + h(f) R_{i,j} \tag{6}$$

where $log\ Y_{ij}(f)$ is the log(base10) of the observed Fourier acceleration amplitude of event i at site j at frequency(f), R_{ij} is the hypocentral distance of site j from the source i, and $h(f)$ is the anelastic attenuation constant for the region (for a given frequency). The level of the curve is set by the event-amplitude term $c_i(f)$. The term 0.5 log R on the left side of the equation adjusts all amplitudes for an assumed geometric spreading of $1/R^{0.5}$, which corresponds to surface-wave spreading in a half-space. In Equation (3), anelastic attenuation term has the following relationship with $Q(f)$:

$$h(f) = \frac{-\pi f}{2.3 \beta Q(f)} \tag{7}$$

β is considered equal to 3.4 in the region (Taghizadeh-Farahmand et al., 2010). Using this preliminary $h(f)$, which is based on the regression of the regional data to Equation 6, the geometrical spreading term at close distances is estimated. Therefore, we do the regression on the following Equation for data at all distances (assuming $Z(R)=(1/R)^b$ at close distances):

$$\log Y_{ij}(f) = \begin{cases} c_i(f) - b \log R_{ij} + h(f) R_{ij} \\ R \leq 60km \\ c_i(f) - b \log R_{ij} - 0.5 \log(\frac{R_{ij}}{60}) + \\ h(f) R_{ij} \ \ R > 60km \end{cases} \tag{8}$$

Table 2 and Figure 7 show estimated values of b in Equation (8). The results are very interesting. The coefficient of geometrical spreading for whole range of frequencies considered in this study, averages to 0.9. This is below the usually assumed value for close distances. However, the coefficient of geometrical spreading could be quite different if another range of frequencies is considered. For instance, in the range of 0.4 to 13 Hz, a range that is used by a number of studies in Iran like Hassani et al. (2011) and Zafarani et al. (2011), it averages to 0.99, which is in agreement with those studies. For the range of 1 to 10 Hz, the range of engineering significance, it's even higher (1.04). Consequently, it is concluded that there is an obvious dependency of geometrical spreading on frequency.

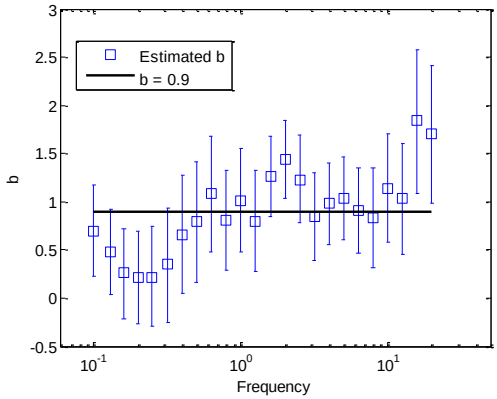

Fig. 7. Estimated values for b (geometrical spreading in close distances) with their 90% lower and upper confidence intervals for the coefficient estimates from the regression (blue bars). Solid black line denotes the average value of geometrical spreading in close distances (b=0.9).

b has an average of 0.9 for the range of frequency in this study, but its value deviates grossly from average in lower and upper edges of the frequencies. Some studies (Atkinson, 2004; Motaghi and Ghods, 2012; Atkinson and Boore, 2014) reported higher values for coefficient of geometrical spreading (bigger than 1); nevertheless, our results based on the available database shows that this is true only if higher frequencies are considered. It might be useful to point out that based on finite fault modeling simulations of strong ground motion in Iran and comparison of the results with ground motion prediction equations (GMPEs), it has been shown that geometrical spreadings with rates higher than 1 may not be appropriate for the region (Samaei et al., 2014).

It is concluded that if a frequency independent geometrical spreading is required to be estimated, the following form would be efficient:

$$Z(R)=\begin{cases}\left(\frac{1}{R}\right)^{0.9} & R\le 60km\\ \frac{1}{60}\left(\frac{60}{R}\right)^{0.5} & R>60km\end{cases} \quad (9)$$

In the next step, based on the geometrical spreading of Equation (9), a regression on equation 8 is performed again but this time to estimate *h(f)* and subsequently the final *Q(f)* (appropriate for all distances).

The results of estimated *Q(f)* values based on this final regression are shown in Figure 8; a least squared fit to the estimated values is also shown. Based on this fit, the following form of quality factor for the studied events is proposed:

$$Q(f)=148f^{0.62} \quad (10)$$

Figure 9 shows the residuals based on this final regression; it is seen that there is no discernable trend in the residuals when plotted against distance.

To show that the estimated attenuation parameters are appropriate for horizontal components, the model (source and path terms) for vertical component database is played back on horizontal component database. The behavior of residuals are also checked. If no important trend in the behavior of residuals is recognized, it will be concluded that the model is valid for horizontal components. This would also mean that H/V ratios are independent of distance.

The residuals after applying the model on horizontal component database are shown in Figure 10. A fitted line is also shown on these plots to evaluate the significance of the trends in distance. There are three negative and one positive distance trends to the residuals of Figure 10, but all the slopes have low values (10^{-4}R and 10^{-5}R). Therefore, we deduce that the attenuation model obtained for vertical components is also applicable for horizontal components. Note that residuals of Figure 10 have positive values at most frequencies, as there are site effects (in form of amplification) for horizontal components.

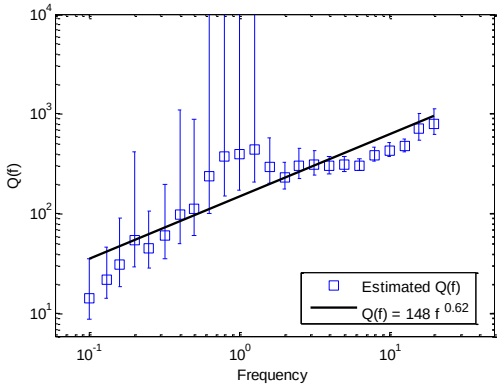

Fig. 8. Estimated values for *Q(f)* with their 90% lower and upper confidence intervals for the coefficient estimates from the regression (blue bars). Solid black line shows the least squared fit to the estimated values.

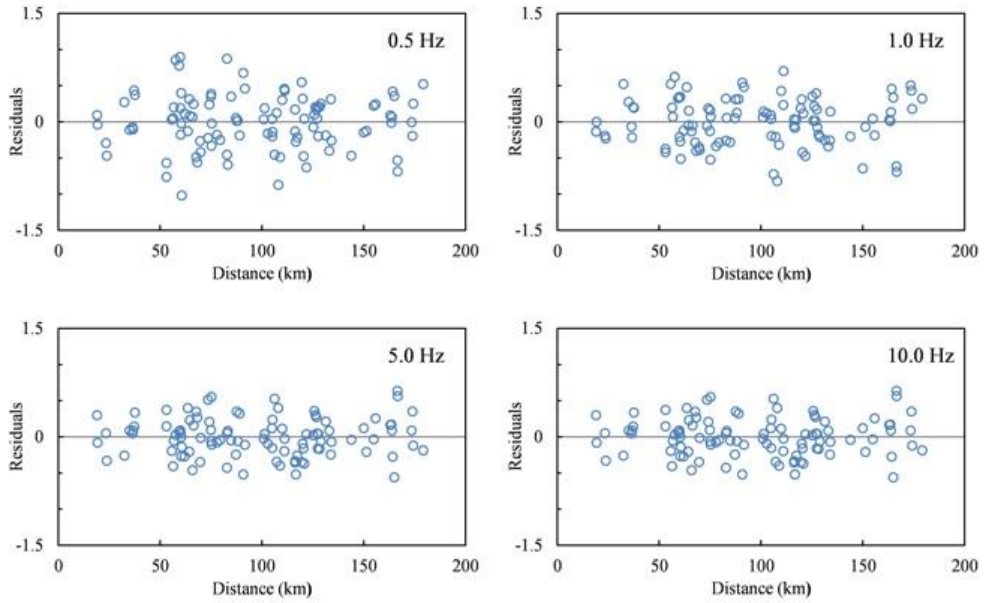

Fig. 9. The residuals for final regression based on Equation 8(in order of estimating *Q(f)*)

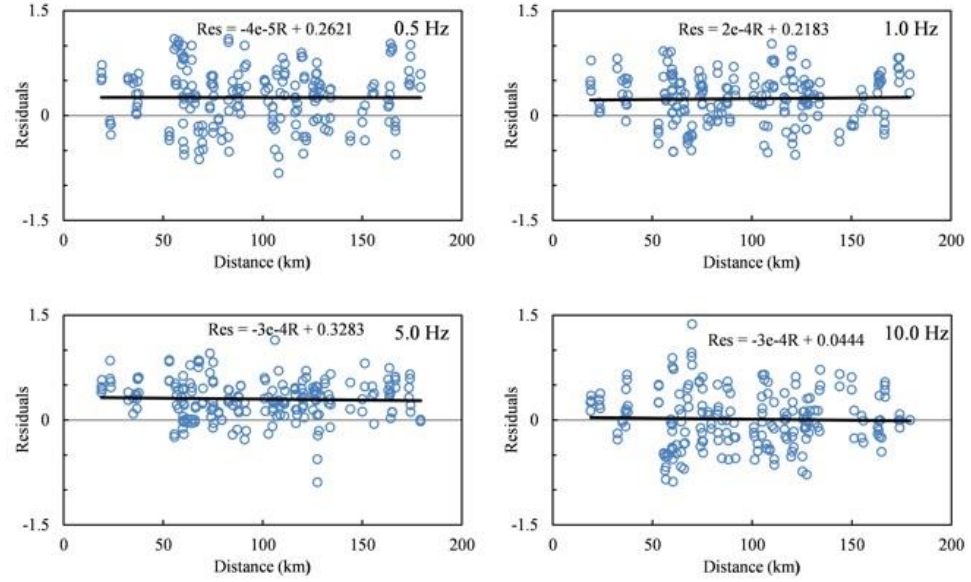

Fig. 10. The residuals for applying the attenuation model of vertical components on horizontal components

5. Comparison with other models

It would be interesting to draw a comparison between the attenuation model obtained in this study and the other models developed for Iran. Table 3 lists most of major studies concerned with developing attenuation for Fourier spectra in Iran along with the one presented in this study. Figure 11 makes a preliminary comparison between the quality factor obtained in this study with that of other studies. It is observed that the estimated quality factor is in the range of other studies for the region. It is also noticed that our model is the only one to cover very low frequencies. However, as there are trade-offs between geometrical spreading and quality factor, it would be more appropriate to compare the attenuation models as a whole. The attenuation model would be *P(f,R)* in Equation (1). Such a comparison is made in Figure 12. The following pointes are noted:

- Variations among the models are low at close distances and high at far distances. This variation is more pronounced at higher frequencies. However, Tsurugi's (2013) model grossly falls below all other models at all distances and all frequencies; this might

be because he has only used few small events that have been recorded at close distances.

- Most of the models have little differences at distances smaller than 60 km, as they all use the same rate of geometrical spreading (i.e. 1). Two dissimilar models are Motaghi and Ghods (2012) with higher and the obtained model in this study with lower rate. Geometrical spreadings with the rates higher than 1 have been reported for smaller events but for bigger events the ambiguities still exist (Boore et al., 2010). It is pointed out that Motaghi and Ghods (2012) have only used small events.
- At long distances, the two models are considerably different from all other models and they propose much higher amplitudes. These are the models developed by Motazedian (2006) and Meghdadi and Shoja-Taheri (2014). Stochastic simulations based on Motazedian's (2006) model have shown over-prediction of this model at great distances (Samaei et al., 2014).

In short, it is concluded that the proposed model in this study is in general agreement with other models, in spite of small differences at low frequencies at close distances. These differences should be further evaluated by attempting to reproduce the observed strong ground motion data using simulations.

Table 2. Estimated values for geometrical spreading coefficient for close distances with their 90% lower and upper confidence intervals for the coefficient estimates by the regression

Frequency	b	Upper confidence band	Lower confidence band
0.10	**0.70**	**1.18**	**0.23**
0.13	**0.48**	**0.92**	**0.04**
0.16	**0.26**	**0.72**	**-0.21**
0.20	**0.22**	**0.70**	**-0.26**
0.25	**0.22**	**0.74**	**-0.29**
0.32	**0.35**	**0.94**	**-0.25**
0.40	**0.66**	**1.27**	**0.05**
0.50	**0.79**	**1.41**	**0.16**
0.63	**1.08**	**1.68**	**0.48**
0.80	**0.81**	**1.33**	**0.29**
1.00	**1.01**	**1.55**	**0.48**
1.26	**0.80**	**1.33**	**0.28**
1.59	**1.26**	**1.68**	**0.84**
2.00	**1.44**	**1.84**	**1.03**
2.52	**1.23**	**1.69**	**0.78**
3.17	**0.84**	**1.30**	**0.39**
3.99	**0.98**	**1.40**	**0.56**
5.02	**1.03**	**1.46**	**0.60**
6.32	**0.91**	**1.35**	**0.47**
7.96	**0.83**	**1.35**	**0.31**
10.02	**1.14**	**1.71**	**0.58**
12.62	**1.03**	**1.60**	**0.45**
15.89	**1.84**	**2.58**	**1.09**
20.00	**1.70**	**2.41**	**0.98**
average	**0.90**		

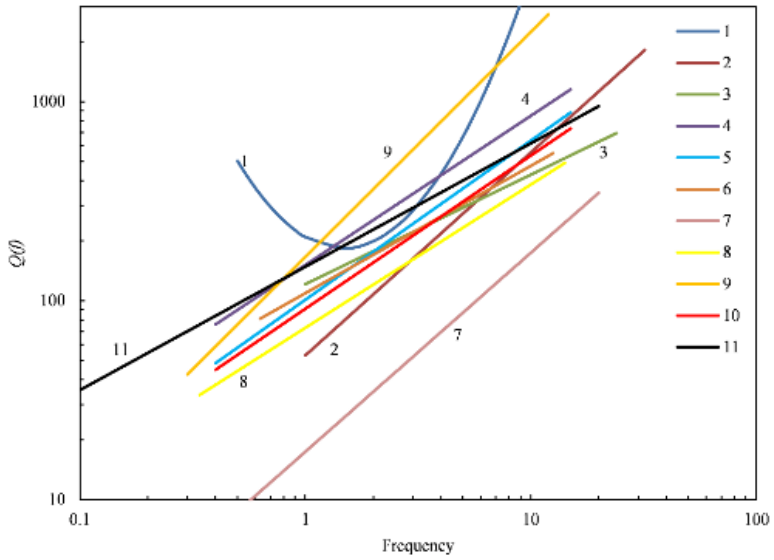

Fig. 11. Comparing the *Q(f)* obtained in this study and those from other studies in the region

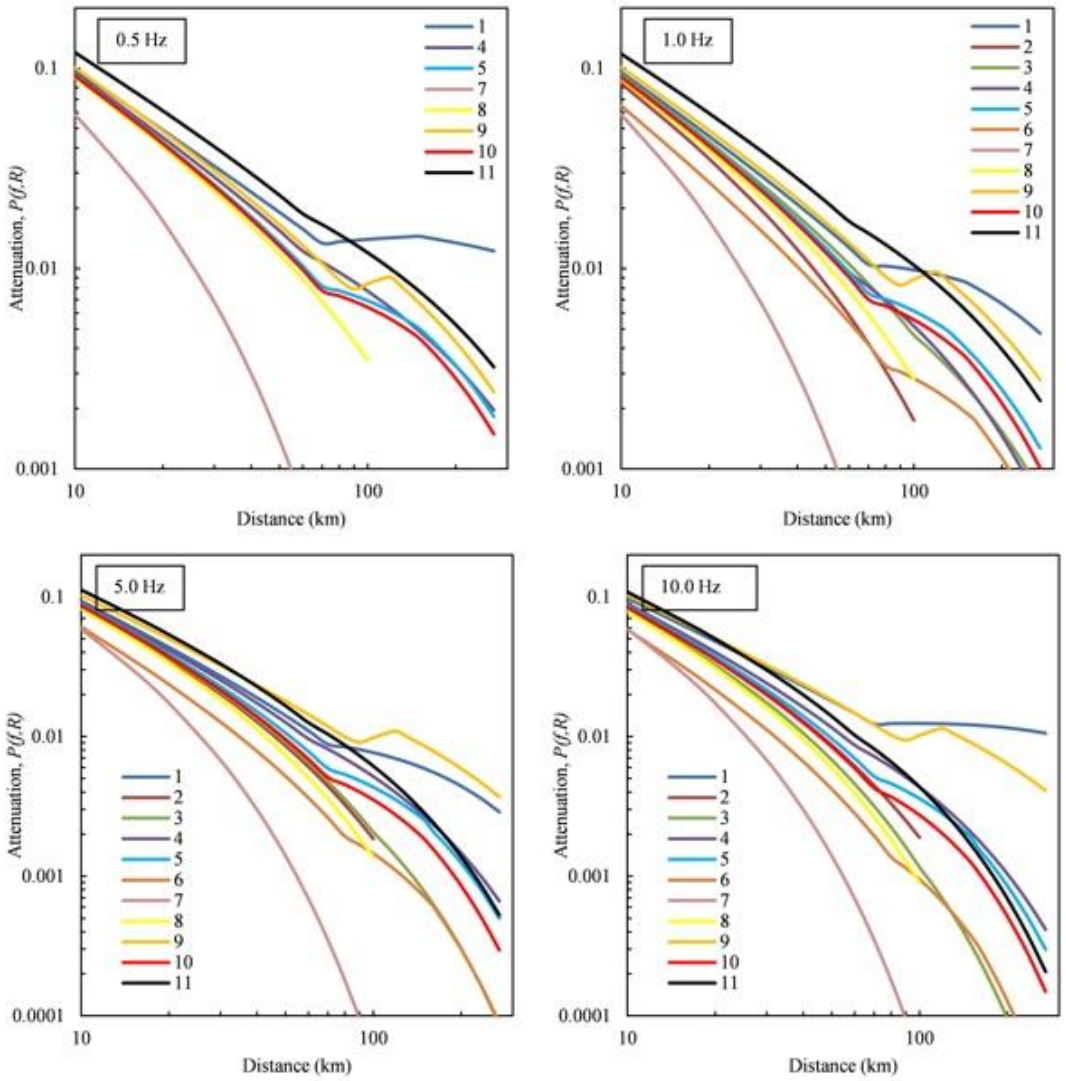

Fig. 12. Comparison of the attenuation model obtained in this study with that of other studies in the region.

Table 3. Major attenuation models presented for Iran

No.	Study	Region	Frequency band	Geometrical spreading	Quality factor
1	Motazedian (2006)	Northern Iran	0.5 – 10 Hz	$R^{-1.0}$(R<70 km) $R^{0.2}$(70≤R≤150 km) $R^{-0.1}$(R>150 km)	$\log Q_S = 1.99(\log f)^2 - 0.67\log f + 2.32$
2	Ma'hood et al. (2009)	East central Iran	1 – 32 Hz	$R^{-1.0}$(R<100 km)	$Q_S = 53 f^{1.02}$
3	Hamzehloo et al. (2010)	Zagros region, Iran	1 – 24 Hz	$R^{-1.0}$(R≤100 km) $R^{-0.5}$(R>100 km)	$Q_S = 121 f^{0.55}$
4	Hassani et al. (2011)	East central Iran	0.4 – 15 Hz	$R^{-1.0}$(R≤60 km) $R^{-0.5}$(R>60 km)	$Q_S = 151 f^{0.75}$
5	Zafarani et al. (2012)	Alborz region, Iran	0.4 – 15 Hz	$R^{-1.0}$(R<70 km) $R^{0.2}$(70≤R≤150 km) $R^{-0.1}$(R>150 km)	$Q_S = 101 f^{0.80}$
6	Motaghi and Ghods (2012)	Alborz region, Iran	0.63 – 12.56 Hz	$R^{-1.15}$(R<80 km) $R^{0.09}$(80≤R≤160 km) $R^{-0.5}$(R>160 km)	$Q_S = 109 f^{0.64}$
7	Tsurugi (2013)	North-western Iran	0.5 – 20 Hz	$R^{-1.0}$(R<100 km)	$Q_S = 17.4 f^{1.00}$
8	Samaei et al. (2013)	Tehran region, Iran	0.34 – 14.13 Hz	$R^{-1.0}$(R<100 km)	$Q_S = 73 f^{0.72}$
9	Meghdadi and Shoja-Taheri (2014)	Eastern Iran	0.3 – 12 Hz	$R^{-0.97}R$<87 km) $R^{0.15}$(87≤R≤119 km) $R^{-0.73}$(R>119 km)	$Q_S = 166 f^{1.13}$
10	Zafarani et al. (2015)	North-western Iran	0.4 – 15 Hz	$R^{-1.0}$(R<70 km) $R^{0.2}$(70≤R≤150 km) $R^{-0.1}$(R>150 km)	$Q_S = 91 f^{0.77}$
11	This study	North-western Iran	0.1 – 20 Hz	$R^{-0.9}$(R≤60 km) $R^{-0.5}$(R>60 km)	$Q_S = 148 f^{0.62}$

5. Conclusions

We used 102 three component recordings of 2012 Ahar-Varzaghan double earthquakes (Mw=6.5, 6.3) to study the attenuation form of Fourier spectra of these two events. In searching for an optimal bilinear shape of geometrical spreading, we used a nonparametric regression on the data and found that the hinge point is at distance of about 60 km from the source. With the well accepted geometrical spreading of $R^{-0.5}$ at regional distances, we estimated preliminary anelastic attenuation and used it to estimate the rate of geometrical spreading at close distances. It was found that the rate of geometrical spreading is noticeably dependent on the considered frequency band. Although for higher frequencies the decay may have a slope steeper than R^{-1}, this is not the case for lower frequencies. Our analysis indicates that for frequencies logarithmically spaced between 0.1 and 20 Hz, geometrical spreading is $R^{-0.9}$. Using this geometrical spreading at close distances, we estimated anelastic attenuation and quality factor, *Q(f)*, subsequently. The estimated *Q(f)* in this study agrees well with the other estimated shear wave quality factors in the region. However, some differences are seen if the whole attenuation model (consisted of anelastic attenuation and geometrical spreading) is considered.

Acknowledgments

We benefited greatly from the discussion with David Boore about data processing; he kindly did some sample processing on our database. Azad Yazdani reviewed the paper and made helpful comments. Three anonymous reviewers also provided useful remarks and corrections that helped improve the manuscript. We finally thank Building and Housing Research Center (BHRC) for providing us with the data, especially Esmaeil Farzangan who answered our many questions about the stations. Strong motion record processing and calculation of FAS in this article were done mostly by TSPP (Boore, 2008) and partly by USDP (Akkar, 2008).

References

Akkar, S., 2008, An introduction to utility software for data processing (USDP), in 4th BSHAP Project Workshop, Budva, Montenegro.

Akkar, S. and Bommer, J. J., 2006, Influence of long-period filter cut-off on elastic spectral displacements, Earthquake Engineering & Structural Dynamics, 35(9), 1145-1165.

Allen, T. I., Cummins, P. R., Dhu, T. and Schneider, J. F., 2007, Attenuation of ground-motion spectral amplitudes in

Southeastern Australia, Bulletin of the Seismological Society of America, 97(4), 1279-1292.

Anderson, J. G. and Hough, S. E., 1984, A model for the shape of the Fourier amplitude spectrum of acceleration at high frequencies, Bulletin of the Seismological Society of America, 74(5), 1969-1993.

Atkinson, G. M., 1993, Earthquake source spectra in eastern North America, Bulletin of the Seismological Society of America, 83(6), 1778-1798.

Atkinson, G. M., 2004, Empirical attenuation of ground-motion spectral amplitudes in southeastern Canada andthe northeastern United States, Bulletin of the Seismological Society of America, 94(3), 1079-1095.

Atkinson, G. M., 2012, Evaluation of attenuation models for the Northeastern United States/Southeastern Canada, Seismological Research Letters, 83(1), 166-178.

Atkinson, G. M., Assatourians, K., Boore, D. M., Campbell, K. and Motazedian, D., 2009, A guide to differences between Stochastic point-source and Stochastic finite-fault simulations, Bulletin of the Seismological Society of America, 99(6), 3192-3201.

Atkinson, G. M. and Boore, D. M., 1995, Ground-motion relations for eastern North America, Bulletin of the Seismological Society of America, 85(1), 17-30.

Atkinson, G. M. and Boore, D. M., 2014, The attenuation of Fourier amplitudes for rock sites in Eastern North America, Bulletin of the Seismological Society of America, 104(1), 513-528.

Atkinson, G. M. and Mereu, R. F., 1992, The shape of ground motion attenuation curves in southeastern Canada, Bulletin of the Seismological Society of America, 82(5), 2014-2031.

Atkinson, G. M. and Silva, W., 2000, Stochastic modeling of California ground motions, Bulletin of the Seismological Society of America, 90(2), 255-274.

Babaie Mahani, A. and Atkinson, G. M., 2012, Evaluation of functional forms for the attenuation of small-to-moderate-earthquake response spectral amplitudes in North America, Bulletin of the Seismological Society of America, 102(6), 2714-2726.

Beresnev, I. A., Atkinson, G. M., Johnson, P. A. and Field, E. H., 1998, Stochastic finite-fault modeling of ground motions from the 1994 Northridge, California, earthquake. II. Widespread nonlinear response at soil sites, Bulletin of the Seismological Society of America, 88(6), 1402-1410.

Boatwright, J., Fletcher, J. B. and Fumal, T. E., 1991, A general inversion scheme for source, site, and propagation characteristics using multiply recorded sets of moderate-size earthquakes, Bulletin of the Seismological Society of America, 81(5), 56 pp.

Boore, D. M., 1983, Stochastic simulation of high-frequency ground motions based on seismological models of the radiated spectra, Bulletin of the Seismological Society of America, 73(6A), 1865-1894.

Boore, D. M., 1999, Effect of baseline corrections on response spectra for two recordings of the 1999 Chi-Chi, Taiwan, earthquake, in Geological Survey, Open-File Report, 37.

Boore, D. M., 2001, Effect of baseline corrections on displacements and response spectra for several recordings of the 1999 Chi-Chi, Taiwan, earthquake, Bulletin of the Seismological Society of America, 91(5), 1199-1211.

Boore, D. M., 2003, Simulation of ground motion using the stochastic method, Pure and applied Geophysics, 160(3-4), 635-676.

Boore, D. M., 2005, SMSIM---Fortran programs for simulating ground motions from earthquakes: Version 2.3---A Revision of OFR 96-80-A", in US Geological Survey open-file report, 59.

Boore, D. M., 2008, TSPP—A collection of FORTRAN programs for processing and manipulating time series, US Geological Survey open-file report, 1111(56), 154-1782.

Boore, D. M., 2012, Updated determination of stress parameters for nine well-recorded earthquakes in Eastern North America, Seismological Research Letters, 83(1), 190-199.

Boore, D. M. and Bommer, J. J., 2005, Processing of strong-motion accelerograms: needs, options and

consequences, Soil Dynamics and Earthquake Engineering, 25(2), 93-115.

Boore, D. M., Campbell, K. W. and Atkinson, G. M., 2010, Determination of stress parameters for eight well-recorded earthquakes in Eastern North America, Bulletin of the Seismological Society of America, 100(4), 1632-1645.

Boore, D. M., Joyner, W. B. and Fumal, T. E., 1997, Equations for estimating horizontal response spectra and peak acceleration from western North American earthquakes: a summary of recent work, Seismological Research Letters, 68(1), 128-153.

Boore, D. M., Stephens, C. D. and Joyner, W. B., 2002, Comments on baseline correction of digital strong-motion data: examples from the 1999 Hector Mine, California, earthquake, Bulletin of the Seismological Society of America, 92(4), 1543-1560.

Brune, J. N., 1970, Tectonic stress and the spectra of seismic shear waves from earthquakes, Journal of Geophysical Research, 75(26), 4997-5009.

Brune, J. N., 1971, Tectonic stress and the spectra of seismic shear waves from earthquakes: correction, Journal of Geophysical Research, 76(5002),

Castro, R., Anderson, J. and Singh, S., 1990, Site response, attenuation and source spectra of S waves along the Guerrero, Mexico, subduction zone, Bulletin of the Seismological Society of America, 80(6A), 1481-1503.

Chiou, B., Darragh, R., Gregor, N. and Silva, W., 2008, NGA project strong-motion database, Earthquake Spectra, 24(1), 23-44.

Cleveland, W. S., 1979, Robust locally weighted regression and smoothing scatterplots, Journal of the American Statistical Association, 74(368), 829-836.

Cleveland, W. S., 1993, Visualizing data, Hobart Press.

Darragh, B., Silva, W. and Gregor, N., 2004, Strong motion record processing for the PEER center, in Proceedings of COSMOS Invited Workshop on Strong-Motion Record Processing, Richmond, Calif, USA, 26-27.

Hamzehloo, H., Rahimi, H., Sarkar, I., Mahood, M., Alavijeh, H. M. and Farzanegan, E., 2010, Modeling the strong ground motion and rupture characteristics of the March 31, 2006, Darb-e-Astane earthquake, Iran, using a hybrid of near-field SH-wave and empirical Green's function method, Journal of Seismology, 14(2), 169-195.

Hassani, B., Zafarani, H., Farjoodi, J. and Ansari, A., 2011, Estimation of site amplification, attenuation and source spectra of S-waves in the East-Central Iran, Soil Dynamics and Earthquake Engineering, 31(10), 1397-1413.

Herrmann, R. B. and Kijko, A., 1983, Modeling some empirical vertical component Lg relations, Bulletin of the Seismological Society of America, 73(1), 157-171.

Iran Strong Motion Network (ISMN) homepage. [Last accessed May 2014]; Available from: www.bhrc.ac.ir/Portal/ISMN

Iranian Seismological Center (IRSC) homepage. [Last accessed May 2014]; Available from: http://irsc.ut.ac.ir/

Joyner, W. B. and Boore, D. M., 1981, Peak horizontal acceleration and velocity from strong-motion records including records from the 1979 Imperial Valley, California, earthquake, Bulletin of the Seismological Society of America, 71(6), 2011-2038.

Lermo, J. and Chávez-García, F. J., 1993, Site effect evaluation using spectral ratios with only one station, Bulletin of the Seismological Society of America, 83(5), 1574-1594.

Ma'hood, M., Hamzehloo, H. and Doloei, G. J., 2009, Attenuation of high frequency P and S waves in the crust of the East-Central Iran, Geophysical Journal International, 179(3), 1669-1678.

Macias, M., Atkinson, G. M. and Motazedian, D., 2008, Ground-Motion Attenuation, Source, and SiteEffects for the 26 September 2003 M 8.1 Tokachi-Oki earthquake sequence, Bulletin of the Seismological Society of America, 98(4), 1947-1963.

Meghdadi, A. and Shoja-Taheri, J., 2014, Ground-motion attenuation and source spectral shape for earthquakes in Eastern Iran, Bulletin of the Seismological Society of America, 104(2), 624-633.

Mirzaei Alavijeh, H., Sinaiean, F., Farzanegan, E. and Sadeghi Alavijeh, M., 2007, Iran strong motion network (ISMN) prospects and achievements, in Proceedings of the 5th International Conference on Seismology and Earthquake Engineering, Tehran.

Motaghi, K. and Ghods, A., 2012, Attenuation of ground-motion spectral amplitudes and its variations across the Central Alborz Mountains, Bulletin of the Seismological Society of America, 102(4), 1417-1428.

Motazedian, D., 2006, Region-specific key seismic parameters for earthquakes in Northern Iran, Bulletin of the Seismological Society of America, 96(4A), 1383-1395.

Motazedian, D. and Atkinson, G. M., 2005, Stochastic finite-fault modeling based on a dynamic corner frequency, Bulletin of the Seismological Society of America, 95(3), 995-1010.

Nayak, A., Kumar, Nath, S., Kumar Singh Thingbaijam, K. and Baruah, S., 2011, New insights into path attenuation of ground motions in Northeast India and Northwest Himalayas, Bulletin of the Seismological Society of America, 101(5), 2550-2560.

Raoof, M., Herrmann, R. and Malagnini, L., 1999, Attenuation and excitation of three-component ground motion in southern California, Bulletin of the Seismological Society of America, 89(4), 888-902.

Samaei, M. and Miyajima, M., 2016, Source spectra of 2012 Ahar-Varzaghan double earthquakes, Northwestern Iran, Journal of Seismology and Earthquake Engineering, (In review).

Samaei, M., Miyajima, M., Tsurugi, M. and Fallahi, A., 2013, Source and path parameters for recorded earthquakes in Tehran Province, Iran, Journal of Japan Society of Civil Engineers, Ser. A1 (Structural Engineering & Earthquake Engineering (SE/EE)), 69(4), I_980-I_988.

Samaei, M., Miyajima, M. and Yazdani, A., 2014, Prediction of strong ground motion using Stochastic finite fault method: a case study of Niavaran fault, Tehran, Geodynamics Research International Bulletin, 2(3), 13-23 (In Persian).

Sinaeian, F., Mirzaei Alavijeh, H. and Farzanegan, E., 2010, Site geology investigation in accelerometric stations using seismic refraction method in Ardebil and East Azarbayejan Provinces, Vol. 2, 50 stations, Center of Iran, Tehran, Iran, in BHRC Publication No. R-532, Building and Housing Research.

Street, R. L., Herrmann, R. B. and Nuttli, O. W., 1975, Spectral characteristics of the Lg wave generated by central United States earthquakes, Geophysical Journal International, 41(1), 51-63.

Taghizadeh-Farahmand, F., Sodoudi, F., Afsari, N. and Ghassemi, M. R., 2010, Lithospheric structure of NW Iran from P and S receiver functions, Journal of seismology, 14(4), 823-836.

Tsurugi, M., 2013, Strong ground motion prediction for scenario earthquakes, 207-223.

Wang, C. and Herrmann, R., 1980, A numerical study of P-, SV-, and SH-wave generation in a plane layered medium, Bulletin of the Seismological Society of America, 70(4), 1015-1036.

Wang, G.-Q., Boore, D. M., Igel, H. and Zhou, X.-Y., 2003, Some observations on collocated and closely spaced strong ground-motion records of the 1999 Chi-Chi, Taiwan, earthquake, Bulletin of the Seismological Society of America, 93(2), 674-693.

Zafarani, H., Hassani, B. and Ansari, A., 2012, Estimation of earthquake parameters in the Alborz seismic zone, Iran using generalized inversion method, Soil Dynamics and Earthquake Engineering, 42, 197-218.

Zafarani, H., Rahimi, M., Noorzad, A., Hassani, B. and Khazaei, B., 2015, Stochastic simulation of strong-motion records from the 2012 Ahar–Varzaghan Dual earthquakes, Northwest of Iran, Bulletin of the Seismological Society of America.

Zaré, M. and Bard, P.-Y., 2002, Strong motion dataset of Turkey: data processing and site classification, Soil Dynamics and Earthquake Engineering, 22(8), 703-718.